UC Davis

UC Davis Previously Published Works

Title

Nanomedicine for Spontaneous Brain Tumors: A Companion Clinical Trial

Permalink

https://escholarship.org/uc/item/3kv0d8h3

Journal

ACS Nano, 13(3)

ISSN

1936-0851

Authors

Arami, Hamed
Patel, Chirag B
Madsen, Steven J
et al.

Publication Date

2019-03-26

DOI

10.1021/acsnano.8b04406

Peer reviewed

eScholarship.org Powered by the California Digital Library
University of California

Author Manuscript

Author Manuscript

Author Manuscript

Author Manuscript

HHS Public Access

Author manuscript

ACS Nano. Author manuscript; available in PMC 2019 June 19.

Published in final edited form as:

ACS Nano. 2019 March 26; 13(3): 2858–2869. doi:10.1021/acsnano.8b04406.

Nanomedicine for Spontaneous Brain Tumors: A Companion Clinical Trial

Hamed Arami[†], **Chirag B. Patel**[†,‡], **Steven J. Madsen**[§], **Peter J. Dickinson**[‖], **Ryan M. Davis**[†], **Yitian Zeng**[§], **Beverly K. Sturges**[‖], **Kevin D. Woolard**[⊥], **Frezghi G. Habte**[†], **Demir Akin**[†], **Robert Sinclair**[§], and **Sanjiv S. Gambhir**[*,†,§,#,¶]

[†]Department of Radiology, Molecular Imaging Program at Stanford (MIPS), Stanford University School of Medicine, Stanford, California 94305, United States

[‡]Department of Neurology and Neurological Sciences, Stanford University School of Medicine, Stanford, California 94304, United States

[§]Department of Materials Science and Engineering, Stanford University, Stanford, California 94305, United States

[‖]Department of Surgical and Radiological Sciences, University of California at Davis, Davis, California 95616, United States

[⊥]Department of Pathology, Microbiology and Immunology, University of California, Davis, California 95616, United States

[#]Department of Bioengineering, Stanford University, Stanford, California 94305, United States

[¶]Stanford Neuroscience Institute, Stanford University School of Medicine, Stanford, California 94305, United States

Abstract

Nanoparticles' enhanced permeation and retention (EPR) variations due to tumor heterogeneity in naturally occurring brain tumors are commonly neglected in preclinical nanomedicine studies. Recent pathological studies have shown striking similarities between brain tumors in humans and dogs, indicating that canine brain tumors may be a valuable model to evaluate nanoparticles' EPR in this context. We recruited canine clinical cases with spontaneous brain tumors to investigate nanoparticles' EPR in different brain tumor pathologies using surface-enhanced Raman spectroscopy (SERS). We used gold nanoparticles due to their surface plasmon effect that enables their sensitive and microscopic resolution detection using the SERS technique. Raman microscopy of the resected tumors showed heterogeneous EPR of nanoparticles into oligodendrogliomas and meningiomas of different grades, without any detectable traces in necrotic parts of the tumors or

[*]Corresponding Author (Sanjiv S. Gambhir). sgambhir@stanford.edu.

ASSOCIATED CONTENT

Supporting Information

The Supporting Information is available free of charge on the ACS Publications website at DOI: 10.1021/acsnano.8b04406.

Figures providing additional nanoparticle characterization, tissue analysis, and brain MRI and photographs showing administration of the nanoparticles and tumor resection (PDF)

Videos showing the 3D MRI of the brains to localize the tumors in each individual patient (ZIP)

The authors declare no competing financial interest.

Author Manuscript Author Manuscript Author Manuscript Author Manuscript

normal brain. Raman observations were confirmed by scanning electron microscopy (SEM) and X-ray elemental analyses, which enabled localization of individual nanoparticles embedded in tumor tissues. Our results demonstrate nanoparticles' EPR and its variations in clinically relevant, spontaneous brain tumors. Such heterogeneities should be considered alongside routine preoperative imaging and histopathological analyses in order to accelerate clinical management of brain tumors using nanomedicine approaches.

Graphical Abstract

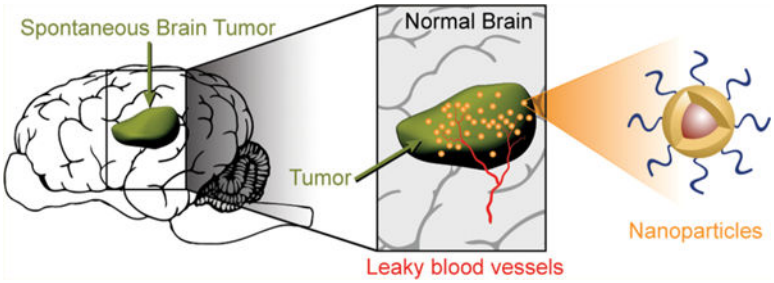

Keywords

clinical trial; nanoparticle; canine; brain tumor; glioma; Raman; gold

Neuroscience and neuro-oncology are growing rapidly in the exploration of mechanisms in the pathogenesis and treatment of various types of brain tumors including gliomas.[1,2] Nanomedicine, on the other hand, offers opportunities for management at different stages of brain tumor development.[3] Intravenous administration of different formulations of nanoparticles such as gold,[4] iron oxide,[5] liposomes,[6] and polymers[7] have been extensively used for efficient detection and treatment of brain tumors in preclinical mouse and rat models. However, most of these studies have failed in early phase clinical trials due to poor delivery of the nanoparticles into brain tumors.[8] This has been due to a wide range of dissimilarities between spontaneous and invasive brain tumors in humans, compared to animal models in immunologically compromised rodents using orthotopic or transgenic approaches.[9,10]

The frequently used orthotopic brain tumor models involve intracranial implantation of the human tumor cells (*i.e.*, xenografts) in a selected brain location in the animal,[11] but oftentimes the resulting tumor's growth pattern and invasiveness differ from those of the original human patient's tumor.[10,12] Human brain tumor xenografts are predominantly homogeneous, whereas human brain tumors are heterogeneous both within an individual patient and also across different patients.[13,14] However, the inability to fully recapitulate spontaneous naturally occurring human brain tumors' genetic heterogeneity and phenotype in a foreign microenvironment is still a major drawback of transgenic models, particularly for nanomedicine-related approaches.[15,16]

The tumor microenvironment (*e.g.,* expression of extracellular matrix proteins), heterogeneity, three-dimensional network of blood vessels and varying vascular permeability, and intracranial pressure are different in rodent models, compared to

Author Manuscript Author Manuscript Author Manuscript Author Manuscript

spontaneously forming brain tumors in humans. Invasion of the tumor into normal brain parenchyma is a key feature in the development of naturally occurring brain tumors,[17] but many of the most commonly used xenografted human brain tumors in rodents, including the U87/MG glioblastoma cell line, form a discrete mass around the implantation site and compress the surrounding normal brain tissues with minimal invasiveness and regional spread.[12] Such variations in the local environment can change the tumor permeation and retention dynamics of nanoparticles in experimental versus spontaneous tumors.[18] Additionally, the faster resting heart rate in rodents (310–840 beats/min in mice and 250–493 beats/min in rats compared to 72 beats/min in humans) and different blood pressure (systolic/diastolic) in rodents (113–160/81–110 mmHg in mice and 84–184/58–145 mmHg in rats compared with 120/80 mmHg in humans)[19] expose nanoparticles to much higher shear stresses on their surface in rodents that likely alters nanoparticle blood stability. This creates discrepancies between nanoparticles' blood clearance pharmacokinetics and hepatic uptake mechanisms, likely requiring redesign of the nanoparticles' physiochemical properties (*e.g.*, size, surface charge, and coating molecules) for clinical applications, even if they successfully pass small animal experiments.[5,20]

In addition to the limiting factors discussed above, the evaluation of nanotherapeutic approaches in rodent models of glioblastoma (GBM, World Health Organization [WHO] grade IV glioma), the most common and lethal form of primary brain cancer, is not realistic because the standard-of-care approach for GBM treatment in humans is surgical resection followed by radiation therapy and temozolomide chemotherapy.[21] The inability to resect an orthotopically implanted human xenograft from the rodent brain accurately and mimic the time course of postresection radiation therapy and chemotherapy leads to this infeasibility of modeling GBM treatment with high fidelity in small animal models.[22] These neglected parameters in rodent models, the high costs of clinical trials, and difficulties in recruiting human patients are the main drawbacks hindering the successful translation of nanomedicine approaches to clinical neuro-oncology.

Nanoparticle delivery depends on EPR in brain tumors.[5,23] However, current understanding of the nanoparticles' EPR in brain tumors is limited, due to differences in blood–brain barrier (BBB) permeability in rodent brain tumor models compared with natural spontaneous brain tumors. Here, we used a high resolution and ultrasensitive approach to evaluate gold nanoparticles' EPR in clinically relevant and naturally occurring spontaneous brain tumors in canine clinical cases (companion animal clinical trial). These models have also been successfully used before for evaluation of convection enhanced diffusion (CED) of intracranially administered nanoparticles[24,25] or drug delivery to brain tumors using other drug carriers such as mini-cells.[26]

Canine spontaneous brain tumors are a valuable model system in which to evaluate the clinical translatability of different brain tumor diagnostic and therapeutic approaches.[27] The prevalence of malignant gliomas (WHO grade III or IV) among pet dogs is comparable to that in humans,[25] and naturally occurring brain tumors in dogs share many of the biological features of their human counterparts.[28] The gross pathological, microscopic, and immunohistochemical features shared between human and canine spontaneous brain tumors include similar anatomical locations, *e.g.*, predominantly cortical or thalamic locations (*i.e.*,

Author Manuscript Author Manuscript Author Manuscript Author Manuscript

supratentorial) for gliomas, with invasion into normal brain tissue, breakdown of the blood–brain barrier, necrosis, cyst formation, and angiogenesis.[29–31] Also, molecular biology analyses of the tumor tissues have shown similar key pathway abnormalities between canine and human brain tumors, particularly in gliomas with involvement of growth factors and TP53 and RB1 pathways.[32–34] The immunologic features associated with human and canine brain tumors also share similarities (*e.g.*, programmed death 1 [PD-1] immunoinhibitory mechanisms[35] and tumor infiltration of macrophages or T cells[36]). The features discussed above are less frequently observed or sometimes absent in rodent human brain tumor xenograft models; moreover, the median survival time scale in orthotopic rodent models of GBM is on the order of 4–8 weeks postimplantation (depending on the cell line being implanted, number of implanted cells, location of implantation, *etc.*,[37] whereas it is 16 months in humans[38] and 7.4 months in dogs.[39]

Our evaluation of nanoparticles' EPR into spontaneous brain tumors is based on the SERS technique, which offers ultrahigh sensitivity, microscopic resolution, and signal specificity with multiplexing capabilities.[40,41] Gold nanoparticles (GNPs) have been extensively used as SERS nanoprobes due to their surface plasmon characteristics, biocompatibility, and facile synthesis.[42,43] Therefore, successful delivery of GNPs to spontaneous brain tumors could be feasibly evaluated by SERS-assisted technologies. The high sensitivity and microscopic resolution of SERS enabled us to monitor the nanoparticles' uptake accurately without additional tagging, which usually changes the physiochemical characteristics of the nanoparticles and might raise regulatory safety concerns. These preliminary results introduce a general platform for more effective and realistic evaluation of nanomedicine approaches for different neuro-oncology applications. This study is based on using a clinically relevant brain tumor model and should help to fill the translational gaps between nanomedicine and neuro-oncology in the near future.

RESULTS AND DISCUSSION

We used canine clinical cases with spontaneously occurring brain tumors for validation of nanoparticles' EPR (Figures 1a and S1). This translational study was designed following our previous publication, reporting successful EPR of these nanoparticles into orthotopic brain tumors in mice.[4] GNPs were used because of their suitability for highly sensitive detection using the SERS approach. The Raman GNPs used in this study consist of a gold core coated with a monolayer of active Raman molecules and a silica shell, which is functionalized with excessive amounts of thiol (–SH) groups (Figure 1b). First, we stabilized the labeled GNPs by conjugation of polyethylene glycol ($MM(PEG)_{12}$) molecules to their surfaces (Figures 1b and S2), as successful nanoparticle delivery to tumors depends on their size stability in blood.[5] PEG molecules had a terminal maleimide group at their backbone structure, and they were effectively conjugated to thiol groups on the surface of GNPs (Figures 1b and S2), by a quick thiolmaleimide reaction.[44] PEGylated GNPs were purified by centrifugation and redispersion in 5% wt/volume dextrose solution (D5W). GNPs were then sterilized in a good manufacturing practice (GMP) facility as standard criteria required for all drugs and reagents used in clinical studies, and the final concentration was adjusted to 0.5–1 nM of GNPs dispersed in D5W. GNP concentration was calculated by measuring their absorption peak

Author Manuscript Author Manuscript Author Manuscript Author Manuscript

intensity at 532 nm compared with absorption intensity of an original stock solution with known concentration.

GNP size, surface charge, and core–shell structure were characterized using dynamic light scattering (DLS), zeta potential, and SEM, respectively. Hydrodynamic size of the GNPs was ~149.5 nm with a polydispersity index (PDI) of 0.06 (Figure 2a). The volume and number percentage modes of the DLS graphs are also shown in Figure S3. Such a low PDI confirms high monodispersity of the PEGylated GNPs. Zeta potential of the GNPs was around −27 ± 5 mV (Figure 2b) due to the presence of silica coating.[45] Secondary electron SEM generally provided more topographical information and showed the gold core with a darker contrast, compared to the brighter silica shell (Figure 2d), because of its higher electron absorption cross section. However, backscattered SEM analysis showed the core gold with a brighter contrast, mainly due to its high electron scattering cross section. These results confirmed the presence of a silica coating with uniform thickness of ~36 ± 4 nm (standard deviation ~ 3.7 nm) around the GNPs, which is also shown in the transmission electron microscopy (TEM) image shown in Figure S4. Both SEM and TEM analyses clearly showed the core–shell structure of the GNPs. This is critical because this silica layer was designed to pack the Raman reporter molecules on the surface of gold and prevent their detachment.[4] A typical Raman spectrum of these PEGylated GNPs (785 nm laser, ~ 21 mW) is also shown in Figure 2c. The characteristic peaks observed at ~1020, 1180, 1330, 1600, and 1630 cm^{-1} were consistently observed in all Raman measurements associated with these GNPs for sensitive detection of the GNPs in brain tumors. These fingerprint peaks were also used for reconstruction of all the Raman microscopy images.

Four clinical dogs with spontaneous brain tumors (Cases 1–4), weighing 8.7–24.7 kg, were prospectively recruited into this study (Table 1). Standard MRI imaging protocols were used to define tumor location and postsurgical extent of resection.[46] As shown in Figure S1, the original solution of gold nanoparticles (GNPs, 0.5 pmol per kg of the body weight) dispersed in D5W solution was first mixed with additional D5W to reach to a final volume of 60 mL. Then the mixture was infused (2 mL/min) via cephalic vein into each dog. Tumors were resected under anesthesia at ~24 h post-GNP infusion (Figure S5, Figure 3). The resected tissues were fixed in 10% buffered formalin and analyzed by surface enhanced Raman spectroscopy (SERS) imaging, hematoxylin and eosin (H&E) histology, inductive coupled plasma mass spectroscopy (ICP-MS), and SEM.

SERS is a feasible technique enabling detection of GNP traces as low as 70 pM, with ultrahigh microscopic resolution (1 μm).[40] Also, as described above, the Raman reporter molecules were originally attached to the gold surface and packed tightly under a stable silica shell. Therefore, using SERS was beneficial because we did not need to do additional fluorescent or gadolinium tagging or radiolabeling. Such labeling is required for other imaging modalities (*i.e.*, fluorescent imaging, MRI, or positron emission tomography [PET], respectively), which can alter the physiochemical properties of the nanoparticles (*e.g.*, hydrodynamic size and surface charge).[5] We used 100 μm-thick tumor sections for Raman analyses, to ensure a detectable number of GNPs embedded in tissues. The 785 nm near-infrared laser used for our Raman analyses easily penetrated through the whole tissue section, ensuring maximum GNP detection sensitivity. A computer-controlled measurement

Author Manuscript Author Manuscript Author Manuscript Author Manuscript

set up was utilized to collect and record microscopic Raman spectra from each individual 50 μm × 50 μm area (with an acquisition time of 1 s per spectrum), over the entire surface of the selected tissue sections. Then, we used MATLAB for analysis of the recorded spectra (see Methods for details) and compared the spectrum obtained from each point with the reference spectrum obtained from original GNPs (Figure 2c). Finally, Raman images of the tissues were reconstructed (Figure 4), based on signal intensities observed at GNP fingerprint peaks in each measurement to map two-dimensional distribution of GNPs in each tumor section.[47]

MRI and histology results relevant to all cases are shown in Figures 3 (transverse T2-weighted [T2W] and T1-weighted [T1W] MRI and 20× magnification histology images) and S6 (sagittal T2W and T1W MRI and 4× magnification histology images). Also see the Supporting Information 3D MRI videos. Raman images of the tumor sections obtained from these four cases are also shown in Figure 4. We did Raman imaging on sections from different parts of the tumors to evaluate EPR of the GNPs through these heterogeneous, spontaneous tumors. Comparison of these Raman images with the respective bright field images (shown on their left side) showed distribution of the GNPs in the tumor sections. ICP-MS analyses of these tissues showed that the amount of the gold nanoparticles accumulated in tumor tissues were in the range of 0.75–1.5% of the injected dose per gram of the tumor tissues. However, it should be noted that ICP-MS numbers represent the total amount of the gold in a selected tumor mass and do not reflect the heterogeneity of the nanoparticles' EPR. Blood samples were collected at 24 h postinfusion in the 4 dogs and ICP and Raman measurements were taken to determine presence of circulating GNPs. We did not observe any traces of GNPs in these blood samples, suggesting that GNPs were already accumulated in tumors or cleared from the blood by the liver and spleen, part of the reticuloendothelial system (RES).[5]

We also performed laboratory tests including blood chemistry, blood coagulation profiles, hematology, and urinalysis before and 5–30 days after GNPs infusion and did not observe any signs of overt toxicity associated with administration of the GNPs based on the veterinary cooperative oncology group–common terminology criteria for adverse events (VCOG-CTCAE).[48] Dog 3 experienced one grade 1 (thrombocytopenia), one grade 2 (alanine aminotransferase [ALT]), and one grade 3 (alkaline phosphatase) adverse event. The preoperative values for Dog 3 were normal platelet counts and elevated ALT and alkaline phosphatase. Therefore, these events were determined by the treating clinician as unlikely to be associated with the SERS nanoparticle intervention. More studies are required in order to ensure clinical safety of these nanoparticles with higher confidence levels, particularly in regard to liver function and blood counts. Unfortunately, only four animals were tested in this study, and we could not include control brain tumor patient dogs that had not received a GNP infusion. Additional dogs were unable to be studied due to the relatively high costs associated with this canine trial.

Case 1 was diagnosed as psammomatous meningioma (WHO grade I). Preoperative postcontrast T1MRI of the brain showed a uniformly and strongly enhancing mass external to the brain parenchyma in the frontal lobe (Figure 3a–d), indicating hypervascularity.[49] The tumor was resected 24 h post-GNP infusion and evaluated separately by its caudal (blue circle, Figure S9) and rostral (red circle, Figure S7) components. Raman imaging of the

Author Manuscript Author Manuscript Author Manuscript Author Manuscript

caudal and rostral components of this tumor demonstrated moderate signal throughout the tissue sections (Figures 4a,b and S7), suggesting relatively uniform EPR through the entire tumor. Postoperative contrast-enhanced T1W MRI demonstrated a gross total resection (Figure 3d).

In order to locate and analyze individual GNPs in tumor tissues, we used secondary and backscattered electron SEM combined with energy dispersive X-ray spectroscopy for elemental analysis. Figure 5a shows SEM of a selected area around a blood vessel in tumor tissue obtained from Case 1 (meningioma). Zooming at the blood vessel edge (blue square) and using different SEM modes, we were able to visualize individual GNPs. The secondary electron image (top) shows red blood cells inside the blood vessel. Backscattered electron images (bottom and insets) helped visualize GNPs as individual bright spots, indicated with red arrows in the inset images. The particles appeared blurred because they were below the surface of the tissue, resulting in additional scattering of the electrons as they penetrated and escaped the sample. At a higher magnification, backscattered SEM (Figure 5b) showed a typical electron image of GNPs embedded inside the tumor in which the core–shell structure of the nanoparticles can be seen. Nanoscale elemental analysis was also performed to confirm the composition of features present in GNPs (Figure 5c). When the electron beam was at an area with several adjacent bright spots (position indicated by the red dot on the image), the spectrum showed characteristic peaks from silicon (Si) and gold (Au) (Si Kα and Au Mα), confirming that these bright spots were indeed the silica-coated GNPs. These Si and Au peaks disappeared (Figure 5d) when the electron beam was shifted away at a distance of 1–2 μm from these bright spots, *i.e.,* GNPs. Note that a small Au signal remained that can be generated by the AuPd conductive coating on the tissue section to prevent charging during SEM examination.

Case 2 was diagnosed as oligodendroglioma (WHO grade II), a primary brain tumor of glial origin that arises most frequently rostrotentorially in humans and dogs.[50,51] Preoperative T2W MRI (Figure 3f) showed absence of vasogenic edema (swelling in the brain due to extravasation of vascular contents into the brain parenchyma) around the frontal/ parietal tumor.[52] The tumor was composed of areas with and without contrast enhancement as seen in Figure 3h, presumably reflecting areas with and without compromised BBB. The region of the tumor with breakdown of the BBB demonstrated contrast-enhancement (*i.e.,* hyperintense), whereas it was not originally T1-hyperintense prior to injection of the contrast agent as seen in Figure 3g. Figure 3i shows the postoperative postcontrast T1W MRI of the brain (24 h after infusion of the GNPs), demonstrating gross total resection. The H&E-stained tumor tissue sections (Figure 3j) showed the classical “fried-egg appearance” of oligodendroglioma cells, in which the histomorphology included a round nucleus with distinct cell borders and semiclear cytoplasm.[53] Raman imaging demonstrated dense signal throughout the tumor tissue section (Figure 4c), compared to moderate signal in another tumor section 500 μm away (Figure 4d), indicating heterogeneous uptake of the GNPs within the same tumor.

Typical Raman spectra observed at selected points in Figure 4a,c,d are shown in Figures S8 and S9. These representative spectra accurately matched the Raman spectrum of the original GNPs (Figure 2c), confirming the presence of at least several GNPs at the selected points, on

Author Manuscript Author Manuscript Author Manuscript Author Manuscript

or inside the tissue. Increasing the acquisition time from 1 to 5, 10, 20, and 50 s clearly accentuated the GNPs characteristic peaks at the selected points (Figure S8a). However, comparison of Raman images of the same tissue section, generated by acquisition times of 1 and 5 s (Figure S8), showed that increasing the acquisition time did not necessarily change the brightness of the images and the accuracy of the GNPs detection. Also, note that increasing the acquisition time dramatically increased the total imaging time up to more than 24 h for scanning a tissue with an approximate 2.5 cm^2 area.

Case 3 was diagnosed as a fibroblastic meningioma (WHO grade I) based on its firmness and composition of spindle cells with indistinct cell boundaries and a sheet-like architecture (Figures 3o, S6m).[54] In particular, the histomorphology of the tumor tissue featured small elongated cells with prominent nucleoli.[54] Figure 3k shows the preoperative T2W MRI scan. The area of peri-tumoral hyperintensity in this images represent vasogenic edema into the brain parenchyma likely resulting from breakdown of the BBB.[55] Figure 3m,n shows the pre- and postoperative contrast-enhanced T1MRIs, respectively, which demonstrate a minimal region of residual contrast enhancement (Figures 3n, S6l) that more likely represents expected postsurgical inflammation than residual tumor. Raman imaging demonstrated mild signal throughout the tumor tissue section (Figure 4e) compared to absent signal in a region of adjacent normal brain tissue (Figure 4f). In particular, H&E confirmed the absence of tumor cells in this normal brain tissue section (Figure S11), supporting the specificity of the Raman signal for the presence of tumor tissue in this case. However, the majority of gliomas are high-grade, characterized by their invasion into the surrounding normal brain tissue. This important feature should be considered in future studies by designing nanoparticles that can reach and target invasive parts of the brain tumors. Unfortunately, the access to normal tissues for further analyses is generally very limited due to ethical concerns during the surgery.

Case 4 was diagnosed as a high-grade anaplastic oligodendroglioma (WHO III). Diagnostic pathology results showed microvascular proliferation and necrosis indicating the heterogeneous nature of this type of tumor (Figures 3t, S6r, and S10c). Figure 3r,s shows the pre- and postoperative contrast-enhanced T1W MRIs, respectively, which demonstrate minimal residual contrast enhancement consistent with a gross total resection (Figures 3s, S6q). Raman imaging demonstrated dense signal throughout the tumor tissue section (Figure 4g) compared to absent signal in a necrotic tissue specimen from the same case (Figures 4h and S10c). The dense Raman signal observed in case 4 is comparable to that of the WHO grade II oligodendroglioma in Case 2, suggesting that oligodendrogliomas of WHO grade II/III may have a greater NP EPR effect compared to WHO grade I meningiomas (Cases 1 and 3). The absence of Raman signal in the necrotic areas of the tissues is consistent with the likely absence of viable blood vessels in these nonperfused areas of the tumor. Also, we observed an overlap between areas with GNPs' Raman signal and proliferating tumor tissues in their H&E stained counterparts (*e.g.*, see Figure S10). Similarly, the absence of signal within the area of adjacent normal brain in case 3 (Figure 4f) suggests that uptake into normal brain or diffusion from adjacent tumor tissue into normal brain is likely to be minimal.

Author Manuscript Author Manuscript Author Manuscript Author Manuscript

Additional qualitative SEM analysis of the GNPs in meningioma and oligodendroglioma tissues are shown in Figures S13 and S14. However, it should be noted that SEM is a surface sensitive technique and cannot locate blood vessels and nanoparticles that are embedded well inside the tissues. Therefore, it is not possible to obtain accurate statistical conclusions from SEM images. Rather, visualization of nanoparticles' diffusion into the tumor interstitium in correlation with an adjacent blood vessel observed on SEM is suggestive in nature. We also did SEM on a selected area of an oligodendroglioma tissue with a high Raman signal intensity and were able to locate nanoparticles in this selected area. We found this tissue spot based on SEM of a large area of the samples using Raman images as our guide. However, in most of the cases, Raman signals are generated from nanoparticles that are embedded inside the tissues and cannot be seen by SEM.

Taken together, the above findings suggest that the preoperative MRI characteristics are not as prognostic as the final pathology in regards to predicting the density of NPs' EPR and, thus, Raman signal, within the tumor bed. For example, in the meningioma cases (Cases 1 and 3), the area of preoperative T1W MRI contrast-enhancement overlapped significantly with the area of T2-bright signal. However, there was also some T2-bright signal outside the tumor margins (Figure 3a,k). On the other hand, in the oligodendroglioma cases (Cases 2 and 4), the region of overlap between the hyperintense areas on the preoperative T2W and contrast-enhanced T1W MRI scans was relatively smaller. The large regions within these tumors that were T2W-bright but lacking contrast-enhanced T1W signal indicated areas with high water content, suggesting intratumoral edema and necrosis. In Cases 2 and 4, the areas of BBB breakdown seen on the postcontrast T1W MR images are not unexpected in higher-grade tumors that have higher proliferative rates. This may explain the increased BBB breakdown at the periphery of the tumor, where it is most actively invading into the surrounding brain parenchyma. Furthermore, the areas of central necrosis seen in Cases 2 and 4 represent areas that have outgrown the available blood supply and therefore have become necrotic. The GNPs' EPR effect would not be expected to manifest in the necrotic regions or normal brain regions, as demonstrated in Figures 4h, S10c, and 4f, respectively. Although this is a small prospective series, the pattern of the Raman signal may vary depending on tumor type or grade (Figure S12), suggesting that the density of the signal may correlate with the grade of the tumor (low-grade vs high-grade), regardless of tumor type (*e.g.*, meningioma or oligodendroglioma). The value of the Raman signal in the assessment of tumor grade or type will require more extensive studies using larger case series. However, if this bears out to be true, then intraoperative Raman could be used to let the surgeon know whether the tumor is high- or low-grade intraoperatively, which could affect the extent of surgical resection. This is currently done with intraoperative pathology, where a fresh tumor sample is frozen and preliminarily analyzed by the pathologist in the operating room to diagnose the type and grade of the tumor, to help the surgeon decide how much more of the tumor to take out, and whether it would be safe to resect more or not.

CONCLUSIONS

We used a clinically relevant canine model to validate the EPR of nanoparticles in spontaneous brain tumors. Raman, SEM, and histology analyses of the tumor tissue sections showed the variable presence of administered GNPs in tumor tissues, confirming their

Author Manuscript Author Manuscript Author Manuscript Author Manuscript

heterogeneous extravasation into spontaneous brain tumors by the EPR mechanism. Raman images were reconstructed from specific Raman spectrum of the GNPs, such that the detected Raman signals represent only the extravasated GNPs without any background signal from tissue. In addition, the gold cores efficiently backscattered electrons, providing high contrast in the backscattered SEM images of the tumor sections. Energy dispersive X-ray spectroscopy also confirmed the presence of GNPs in tumors. Electron microscopy results suggested that GNPs were more frequently found in tissue areas closer to blood vessel walls.

There are dissimilarities and similarities between results in orthotopic tumors in mice and spontaneous tumors in canine models. GNPs were seen in both tumor models, confirming their EPR effect. However, unlike the orthotopic tumor model in mice, the naturally occurring spontaneous canine tumors were heterogeneous (similar to human tumors), and this resulted in variable EPR of the GNPs. Use of spontaneously occurring large animal tumors with a naturally developing blood/tumor/brain microenvironment is likely to provide additional clinically relevant translational data beyond primary studies in rodent model systems. Moreover, the size of the dog tumor model allowed for translational assessment of clinically relevant factors including delivery of large volumes of infusate and assessment of associated adverse event sequelae as well as assessment of nanoparticle delivery within the context of surgical resection. Even though we only tested nontherapeutic gold/silica nanoparticles in this study, we believe these promising results generally foreshadow clinical applications of nanomedicine in management of human brain tumors. Similar studies are required to investigate and optimize the effects of size and surface charge of the nanoparticles for higher uptake by spontaneous brain tumors at different stages of tumor development. Also, addition of contrast agents compatible with alternative imaging modalities (such as gadolinium for T1MRI or radiotracers for positron emission tomography, PET) to nanoparticles can facilitate their pharmacokinetics and biodistribution studies or provide opportunities for image-guided intraoperative applications in future investigations. These factors together further support using the clinically relevant canine brain tumor model to evaluate the translatability of nanomedicine approaches for the diagnosis and treatment of brain tumors, prior to human clinical trials. Although such canine companion models are more costly compared with orthotopic rodent models, the data generated from them are more likely to be translatable to human patients due to their spontaneously occurring nature.

METHODS

Nanoparticle Preparation and Characterizations.

Nanoparticles used in this study were prepared according to standards of Good Manufacturing Practices (GMP) to ensure their safety and sterility for clinical use. Silica-coated gold nanoparticles (Oxonica S440 with *trans*-1,2-bis(4-pyridyl)-ethylene or BPE as Raman reporter molecule on the surface of gold[40]) were modified and used for this trial as follows: Monodisperse gold nanoparticles had a layer of Raman reporter molecules attached to their surface. A silica (SiO_2) shell with a uniform thickness of ~36 ± 4 nm was also incorporated around each individual nanoparticle to prevent detachment of these Raman reporter molecules from the gold surface. The external surface of this silica layer was also

Author Manuscript Author Manuscript Author Manuscript Author Manuscript

thiolated to provide active thiol groups for covalent bonding of desired molecules to functionalize the nanoparticles.

We coated these nanoparticles with methyl-(PEG)12-maleimide (Thermo Fisher #22711) to stabilize them in aqueous solutions by preventing their aggregation. Briefly, methyl-$(PEG)_{12}$-maleimide was added in at final concentration of 0.6 mM in 1 nM nanoparticles in 10 mM 3-(*N*-morpholino) propanesulfonic acid (MOPS) buffer (pH 7.4). The mixture was stored at room temperature for 3 h followed by spin purification to remove unbound PEG molecules. For purification, the mixture was centrifuged at 2000 rcf for 10 min to precipitate all the nanoparticles. The supernatant was removed, and the pellet was dispersed in D5W solution (5% dextrose in water). This purification step was repeated four additional times. Finally, the nanoparticles were sterilized by 30 min sonication followed by filtration using 200 μm polyvinylidene difluoride (PVDF) membrane syringe filters.

Nanoparticle hydrodynamic size and zeta potential (surface charge) were measured using a Malvern Dynamic Light Scattering (DLS, Westborough, MA) system. The absorption peak of the nanoparticles at 532 nm was also measured with a Thermo Scientific NanoDrop spectrophotometer (Wilmington, DE) and used to determine the concentration of the nanoparticles. A Renishaw Raman microscope (Chicago, IL) was used to monitor the Raman spectra of the nanoparticles.

Patient Recruitment.

All the standard of care procedures used in this study were performed under the operating policies of Veterinary Medical Training Hospital (VMTH) at the University of California at Davis School of Veterinary Medicine. All procedures and protocols were approved by the UC Davis Veterinary Medical Clinical Trials Review Board and Institutional Animal Care and Use Committee. Canine patients were enrolled based on demographic characteristics, history, and MR imaging consistent with a primary intracranial brain tumor. Four dogs with different types of brain tumors were selected for these studies, and details related to each case are provided in Table 1.

Canine Brain MRI.

Images were acquired using a 1.5 T MRI system (GE Signa, GE Healthcare, Waukesha, WI) and a variety of radiofrequency/receiver coils depending on body weight and size. Specific imaging sequences consisted of noncontiguous 3.0 mm thickness transverse slices with a 0.3 mm interslice gap. Specific pulse sequence parameters for T1W imaging were as follows: repetition time (ms) ~ 516.6–1050; echo time (ms) ~ 8.9–16.92; number of excitations, 4; echo train length, 3. Pulse sequence parameters for T2W imaging were as follow: repetition time (ms) ~ 5000; echo time (ms) ~ 97.7–104.6; number of excitations, 3; echo train length, 23. Postgadolinium contrast images were acquired with T1 weighting after administration of 0.1 mmol/kg gadopentetate dimeglumine (0.5 mmol/mL) (Magnevist Bayer HealthCare, Whippany, NJ).

Author Manuscript Author Manuscript Author Manuscript Author Manuscript

Nanoparticle Infusion.

Nanoparticles were infused 18–24 h prior to surgery (Figure S1). Animals were premedicated with diphenhydramine (2 mg/kg body weight, subcutaneously) 20 min before the infusion to reduce the risk of allergic responses. Nanoparticle stock solutions (concentrations 0.5–1 nM) were first reconstituted from sterile vials that were individually prepared for each dog, using additional sterile D5W solution to have 0.5 pmol per kg of the body weight in a total volume of 60 mL. For example, for a dog with X kg weight, we mixed nanoparticle solution containing X pmol of the GNPs with additional D5W to reach to a total volume of 60 mL for each dog, regardless of their weight. Note that 60 mL was the value approved in our protocol. Then, each nanoparticle solution was infused over 30 min (2 mL/min) intravenously, using a syringe pump and a catheter previously placed into the cephalic vein under aseptic conditions. Animals were monitored for adverse events, including neurological deterioration and evidence of anaphylaxis including urticaria, hypotension, tachycardia, and shock during the infusion period and then hourly for 5 h. Blood samples (~10 mL) were also collected aseptically per standard VMTH protocols using peripheral venipuncture.

Brain Tumor Resection Surgery.

Tumor tissues were resected from each dog's brain as part of the standard-of-care surgery and radiation therapy protocols for management of intracranial tumors (Figure S5). Anesthesia was provided by a VMTH anesthesiologist. Specific surgical procedures for tumor resection, surgical closure, and postoperative care including analgesia and sedation were determined by the VMTH neurosurgeons on an individual case basis following standard VMTH protocols for the Neurology/Neurosurgery services.

Laboratory Tests.

Blood (10 mL) and urine (3–5 mL) samples were collected on the day before and 5–30 days after GNPs infusion and surgical resection of the tumors for serum chemistry, coagulation, hematology, and urine analyses. Postinfusion times for sample collections were determined based on clinical status of each case as follows: 5 days for dogs 2 and 4; 7 days for dog 3; and 30 days for dog 1. Adverse events associated with GNP administration were defined using the veterinary cooperative oncology group common terminology criteria for adverse events.[48] Where animals had preexisting abnormalities, adverse events were defined by increase in specific adverse event grade as per VCOG-CTCAE definitions.

Tumor Histology.

Tissue sections were processed and embedded for routine paraffin sectioning. Tissue sections were cut at 5 μM thickness on a rotary microtome (Leica, Sarasota, FL) and stained for routine hematoxylin and eosin (H&E) using an autostainer (Dako). Sections were visualized with a clinical microscope (Olympus Bx-43, Center Valley, PA), and representative images were obtained at 4× and 20× magnifications using an Olympus DP-72 camera using CellSens acquisition software (Olympus).

Author Manuscript Author Manuscript Author Manuscript Author Manuscript

Analysis of the Nanoparticles in Tumor Tissues.

Postsurgery tissues were fixed in 10% buffered formalin and then transferred to 30% sucrose solutions. Sunken tissues indicated cryopreservation, and they were embedded in optimal cutting temperature (OCT) compound, followed by frozen sectioning using a microtome. Adjacent 20 and 100 μm thick sections were cut and placed on separate frosted glass and quartz (Ted Pella Inc., Redding, CA) microscope slides, respectively. The 20 μm thick sections were stained with H&E for comparative histology. Images were acquired at 20× magnification using a NanoZoomer 2.0-RS whole slide imager (Hamamatsu, Japan) and saved as TIFF files using the NanoZoomer Digital Pathology (NDP) Scan version 2.5 software. The 100 μm thick sections were used for Raman analyses by a customized InVia Renishaw microscope with a semiconductor diode near-infrared 785 nm (21 mW power, 20× Olympus objective) laser as the excitation source. This microscope system was equipped with a piezo-controlled stage for micrometer-resolved spatial mapping and a 1 in. CCD detector for spectral resolution of 1.07 cm^{-1}. A computer-controlled translation stage was used to raster-scan the tissues with x–y pixel sizes of 50 μm (acquisition time 1 s). The Raman spectra collected from individual areas of interest were used to construct Raman images, using MATLAB.[47] Briefly, the spectra were modeled as a sum of the pure S440 spectrum and five background principle components obtained from tissue with no nanoparticles. Unmixing was performed pixel-by-pixel by multiplying the measured spectra by the Morse-Penronse pseudoinverse of the forward model matrix. Reconstructed SERS images show the intensity of the S440 component. Concentrations of the gold in nanoparticle solutions and tissues were determined using inductively coupled plasma mass spectroscopy (ICP-MS, Fisher Scientific, Wilmington, DE). ICP samples were prepared according to a method reported before.[56] Finally, tissue sections were sputter coated with a thin layer of AuPd and analyzed using backscattered and secondary electron imaging (SEM, FEI Magellan) and energy-dispersive X-ray spectroscopy (EDS, FEI Helios 600i with EDAX TEAM Octane Plus detector). The electron beams were operated from 5 to 20 kV for secondary and backscattered electron imaging and at 20 kV for spectroscopy.

Supplementary Material

Refer to Web version on PubMed Central for supplementary material.

ACKNOWLEDGMENTS

We acknowledge supports from Stanford Child Health Research Institute (CHRI), Center for Cancer Nanotechnology Excellence for Translational Diagnostics (CCNE-TD), and a NCI-NIH U54 Grant (#1U54CA199075). This work was also supported by NCI-NIH Grant 1R01CA199656–01A1. H.A. was supported by the Stanford Cancer Imaging Training (T32) program (NIH T32 CA009695). C.B.P. was supported by the NIH/NINDS R25 NS065741 Translational Neuroscience Training Grant, Stanford Cancer Institute Fellowship Award for Cancer Research, and American Brain Tumor Association Basic Research Fellowship supported by the Ryan J. Hanrahan Memorial. Part of this work was performed at the Stanford Nano Shared Facilities (SNSF), supported by the National Science Foundation under Award ECCS-1542152. R.M.D. was supported by the Cancer-Translational Nano-technology Training (Cancer-TNT) Program funded by the National Cancer Institute (NCI). We also thank generous funding support from the Ben and Catherine Ivy Foundation.

Author Manuscript Author Manuscript Author Manuscript Author Manuscript

REFERENCES

(1). Mochizuki AY; Frost IM; Mastrodimos MB; Plant AS; Wang AC; Moore TB; Prins RM; Weiss PS; Jonas SJ Precision Medicine in Pediatric Neurooncology: A Review. ACS Chem. Neurosci 2018, 9, 11–28. [PubMed: 29199818]

(2). Langen KJ; Galldiks N; Hattingen E; Shah NJ Advances in Neuro-oncology Imaging. Nat. Rev. Neurol 2017, 13, 279–289. [PubMed: 28387340]

(3). Chakroun RW; Zhang P; Lin R; Schiapparelli P; Quinones-Hinojosa A; Cui H Nanotherapeutic Systems for Local Treatment of Brain Tumors. Wiley Interdiscip Rev. Nanomed Nanobiotechnol 2018, 10, e1479.

(4). Kircher MF; de la Zerda A; Jokerst JV; Zavaleta CL; Kempen PJ; Mittra E; Pitter K; Huang R; Campos C; Habte F; Sinclair R; Brennan CW; Mellinghoff IK; Holland EC; Gambhir SS A Brain Tumor Molecular Imaging Strategy Using a New Triple-modality MRI-photoacoustic-Raman Nanoparticle. Nat. Med 2012, 18, 829–834. [PubMed: 22504484]

(5). Arami H; Khandhar A; Liggitt D; Krishnan KM In Vivo Delivery, Pharmacokinetics, Biodistribution and Toxicity of Iron Oxide Nanoparticles. Chem. Soc. Rev 2015, 44, 8576–8607. [PubMed: 26390044]

(6). Vieira DB; Gamarra LF Getting into the Brain: Liposome-based Strategies for Effective Drug Delivery Across the Blood-brain Barrier. Int. J. Nanomed 2016, 11, 5381–5414.

(7). Nance E; Timbie K; Miller GW; Song J; Louttit C; Klibanov AL; Shih TY; Swaminathan G; Tamargo RJ; Woodworth GF; Hanes J; Price RJ Non-invasive Delivery of Stealth, Brain-penetrating Nanoparticles Across the Blood-brain Barrier Using MRI-guided Focused Ultrasound. J. Controlled Release 2014, 189, 123–132.

(8). Wilhelm S; Tavares AJ; Dai Q; Ohta S; Audet J; Dvorak HF; Chan WCW Analysis of Nanoparticle Delivery to Tumours. Nat. Rev. Mater 2016, 1, 16014.

(9). Lenting K; Verhaak R; Ter Laan M; Wesseling P; Leenders W Glioma: Experimental Models and Reality. Acta Neuropathol 2017, 133, 263–282. [PubMed: 28074274]

(10). Huszthy PC; Daphu I; Niclou SP; Stieber D; Nigro JM; Sakariassen PO; Miletic H; Thorsen F; Bjerkvig R In Vivo Models of Primary Brain Tumors: Pitfalls and Perspectives. Neuro-Oncology 2012, 14, 979–993. [PubMed: 22679124]

(11). Palanichamy K; Patel D; Jacob JR; Litzenberg KT; Gordon N; Acus K; Noda SE; Chakravarti A Lack of Constitutively Active DNA Repair Sensitizes Glioblastomas to Akt Inhibition and Induces Synthetic Lethality with Radiation Treatment in a p53-Dependent Manner. Mol. Cancer Ther 2018, 17, 336–346. [PubMed: 28838997]

(12). Chang E; Pohling C; Natarajan A; Witney TH; Kaur J; Xu L; Gowrishankar G; D'Souza AL; Murty S; Schick S; Chen L; Wu N; Khaw P; Mischel P; Abbasi T; Usmani S; Mallick P; Gambhir SS AshwaMAX and Withaferin A Inhibits Gliomas in Cellular and Murine Orthotopic Models. J. Neuro-Oncol 2016, 126, 253–264.

(13). Soeda A; Hara A; Kunisada T; Yoshimura S; Iwama T; Park DM The Evidence of Glioblastoma Heterogeneity. Sci. Rep 2015, 5, 7979. [PubMed: 25623281]

(14). Inda MM; Bonavia R; Seoane J Glioblastoma Multiforme: a Look Inside its Heterogeneous Nature. Cancers 2014, 6, 226–239. [PubMed: 24473088]

(15). Huse JT; Holland EC Genetically Engineered Mouse Models of Brain Cancer and the Promise of Preclinical Testing. Brain Pathol 2009, 19, 132–143. [PubMed: 19076778]

(16). Simeonova I; Huillard E In Vivo Models of Brain Tumors: Roles of Genetically Engineered Mouse Models in Understanding Tumor Biology and Use in Preclinical Studies. Cell. Mol. Life Sci 2014, 71, 4007–4026. [PubMed: 25008045]

(17). Cha J; Kang SG; Kim P Strategies of Mesenchymal Invasion of Patient-derived Brain Tumors: Microenvironmental Adaptation. Sci. Rep 2016, 6, 24912. [PubMed: 27108713]

(18). Kobayashi H; Watanabe R; Choyke PL Improving Conventional Enhanced Permeability and Retention (EPR) Effects; What Is the Appropriate Target? Theranostics 2014, 4, 81–89.

(19). Milani-Nejad N; Janssen PM Small and Large Animal Models in Cardiac Contraction Research: Advantages and Disadvantages. Pharmacol. Ther 2014, 141, 235–249. [PubMed: 24140081]

Author Manuscript Author Manuscript Author Manuscript Author Manuscript

(20). Chiarelli PA; Revia RA; Stephen ZR; Wang K; Jeon M; Nelson V; Kievit FM; Sham J; Ellenbogen RG; Kiem HP; Zhang M Nanoparticle Biokinetics in Mice and Nonhuman Primates. ACS Nano 2017, 11, 9514–9524. [PubMed: 28885825]

(21). Stupp R; Mason WP; van den Bent MJ; Weller M; Fisher B; Taphoorn MJ; Belanger K; Brandes AA; Marosi C; Bogdahn U; Curschmann J; Janzer RC; Ludwin SK; Gorlia T; Allgeier A; Lacombe D; Cairncross JG; Eisenhauer E; Mirimanoff RO Radiotherapy Plus Concomitant and Adjuvant Temozolomide for Glioblastoma. N. Engl. J. Med 2005, 352, 987–996. [PubMed: 15758009]

(22). Schiff D; Lee EQ; Nayak L; Norden AD; Reardon DA; Wen PY Medical Management of Brain Tumors and the Sequelae of Treatment. Neuro-Oncology 2015, 17, 488–504. [PubMed: 25358508]

(23). Ramanathan RK; Korn RL; Raghunand N; Sachdev JC; Newbold RG; Jameson G; Fetterly GJ; Prey J; Klinz SG; Kim J; Cain J; Hendriks BS; Drummond DC; Bayever E; Fitzgerald JB Correlation between Ferumoxytol Uptake in Tumor Lesions by MRI and Response to Nanoliposomal Irinotecan in Patients with Advanced Solid Tumors: A Pilot Study. Clin. Cancer Res 2017, 23, 3638–3648. [PubMed: 28159813]

(24). Dickinson PJ; LeCouteur RA; Higgins RJ; Bringas JR; Roberts B; Larson RF; Yamashita Y; Krauze M; Noble CO; Drummond D; Kirpotin DB; Park JW; Berger MS; Bankiewicz KS Canine Model of Convection-enhanced Delivery of Liposomes Containing CPT-11 Monitored with Real-time Magnetic Resonance Imaging: Laboratory Investigation. J. Neurosurg 2008, 108, 989–998. [PubMed: 18447717]

(25). Dickinson PJ; LeCouteur RA; Higgins RJ; Bringas JR; Larson RF; Yamashita Y; Krauze MT; Forsayeth J; Noble CO; Drummond DC; Kirpotin DB; Park JW; Berger MS; Bankiewicz KS Canine Spontaneous Glioma: a Translational Model System for Convection-enhanced Delivery. Neuro-Oncology 2010, 12, 928–940. [PubMed: 20488958]

(26). MacDiarmid JA; Langova V; Bailey D; Pattison ST; Pattison SL; Christensen N; Armstrong LR; Brahmbhatt VN; Smolarczyk K; Harrison MT; Costa M; Mugridge NB; Sedliarou I; Grimes NA; Kiss DL; Stillman B; Hann CL; Gallia GL; Graham RM; Brahmbhatt H Targeted Doxorubicin Delivery to Brain Tumors via Minicells: Proof of Principle Using Dogs with Spontaneously Occurring Tumors as a Model. PLoS One 2016, 11, e0151832. [PubMed: 27050167]

(27). Bentley RT; Ahmed AU; Yanke AB; Cohen-Gadol AA; Dey M Dogs Are Man's Best Friend: in Sickness and in Health. Neuro-Oncology 2017, 19, 312–322. [PubMed: 27298310]

(28). LeBlanc AK; Mazcko C; Brown DE; Koehler JW; Miller AD; Miller CR; Bentley RT; Packer RA; Breen M; Boudreau CE; Levine JM; Simpson RM; Halsey C; Kisseberth W; Rossmeisl JH Jr.; Dickinson PJ; Fan TM; Corps K; Aldape K; Puduvalli V; et al. Creation of an NCI Comparative Brain Tumor Consortium: Informing the Translation of New Knowledge from Canine to Human Brain Tumor Patients. Neuro-Oncology 2016, 18, 1209–1218. [PubMed: 27179361]

(29). Bentley RT; Ober CP; Anderson KL; Feeney DA; Naughton JF; Ohlfest JR; O'Sullivan MG; Miller MA; Constable PD; Pluhar GE Canine Intracranial Gliomas: Relationship between Magnetic Resonance Imaging Criteria and Tumor Type and Grade. Vet. J 2013, 198, 463–471. [PubMed: 24051197]

(30). Muscatello LV; Avallone G; Serra F; Seuberlich T; Mandara MT; Siso S; Brunetti B; Oevermann A Glomeruloid Microvascular Proliferation, Desmoplasia, and High Proliferative Index as Potential Indicators of High Grade Canine Choroid Plexus Tumors. Vet. Pathol 2018, 55, 391–401. [PubMed: 29402204]

(31). Herranz C; Fernandez F; Martin-Ibanez R; Blasco E; Crespo E; De la Fuente C; Anor S; Rabanal RM; Canals JM; Pumarola M Spontaneously Arising Canine Glioma as a Potential Model for Human Glioma. J. Comp. Pathol 2016, 154, 169–179. [PubMed: 26804204]

(32). Higgins RJ; Dickinson PJ; LeCouteur RA; Bollen AW; Wang H; Wang H; Corely LJ; Moore LM; Zang W; Fuller GN Spontaneous Canine Gliomas: Overexpression of EGFR, PDGFRalpha and IGFBP2 Demonstrated by Tissue Microarray Immunophenotyping. J. Neuro-Oncol 2010, 98, 49–55.

(33). Dickinson PJ; Roberts BN; Higgins RJ; Leutenegger CM; Bollen AW; Kass PH; LeCouteur RA Expression of Receptor Tyrosine Kinases VEGFR-1 (FLT-1), VEGFR-2 (KDR), EGFR-1,

Author Manuscript Author Manuscript Author Manuscript Author Manuscript

PDGFRalpha and c-Met in Canine Primary Brain Tumours. Vet. Comp. Oncol 2006, 4, 132–140. [PubMed: 19754810]

(34). Dickinson PJ; York D; Higgins RJ; LeCouteur RA; Joshi N; Bannasch D Chromosomal Aberrations in Canine Gliomas Define Candidate Genes and Common Pathways in Dogs and Humans. J. Neuropathol. Exp. Neurol 2016, 75, 700–710. [PubMed: 27251041]

(35). Filley A; Henriquez M; Bhowmik T; Tewari BN; Rao X; Wan J; Miller MA; Liu Y; Bentley RT; Dey M Immunologic and Gene Expression Profiles of Spontaneous Canine Oligodendrogliomas. J. Neuro-Oncol 2018, 137, 469–479.

(36). Boozer LB; Davis TW; Borst LB; Zseltvay KM; Olby NJ; Mariani CL Characterization of Immune Cell Infiltration into Canine Intracranial Meningiomas. Vet. Pathol 2012, 49, 784–795. [PubMed: 21987303]

(37). Chang E; Pohling C; Beygui N; Patel CB; Rosenberg J; Ha DH; Gambhir SS Synergistic Inhibition of Glioma Cell Proliferation by Withaferin A and Tumor Treating Fields. J. NeuroOncol 2017, 134, 259–268. [PubMed: 28681243]

(38). Stupp R; Taillibert S; Kanner A; Read W; Steinberg DM; Lhermitte B; Toms S; Idbaih A; Ahluwalia MS; Fink K; Di Meco F; Lieberman F; Zhu JJ; Stragliotto G; Tran DD; Brem S; Hottinger AF; Kirson ED; Lavy-Shahaf G; Weinberg U; et al. Effect of Tumor-treating Fields Plus Maintenance Temozolomide vs Maintenance Temozolomide Alone on Survival in Patients with Glioblastoma: A Randomized Clinical Trial. JAMA 2017, 318, 2306–2316. [PubMed: 29260225]

(39). Hu H; Barker A; Harcourt-Brown T; Jeffery N Systematic Review of Brain Tumor Treatment in Dogs. J. Vet. Intern. Med 2015, 29, 1456–1463. [PubMed: 26375164]

(40). Zavaleta CL; Smith BR; Walton I; Doering W; Davis G; Shojaei B; Natan MJ; Gambhir SS Multiplexed Imaging of Surface Enhanced Raman Scattering Nanotags in Living Mice Using Noninvasive Raman Spectroscopy. Proc. Natl. Acad. Sci. U. S. A 2009, 106, 13511–13516. [PubMed: 19666578]

(41). Vo-Dinh T; Liu Y; Fales AM; Ngo H; Wang HN; Register JK; Yuan H; Norton SJ; Griffin GD SERS Nanosensors and Nanoreporters: Golden Opportunities in Biomedical Applications. Wiley Interdiscip Rev. Nanomed Nanobiotechnol 2015, 7, 17–33. [PubMed: 25316579]

(42). Smith BR; Gambhir SS Nanomaterials for In Vivo Imaging. Chem. Rev 2017, 117, 901–986. [PubMed: 28045253]

(43). Guerrini L; Graham D Molecularly-mediated Assemblies of Plasmonic Nanoparticles for Surface-enhanced Raman Spectroscopy Applications. Chem. Soc. Rev 2012, 41, 7085–7107. [PubMed: 22833008]

(44). Arami H; Teeman E; Troksa A; Bradshaw H; Saatchi K; Tomitaka A; Gambhir S; Hafeli UO; Liggitt D; Krishnan K Tomographic Magnetic Particle Imaging of Cancer Targeted Nanoparticles. Nanoscale 2017, 9, 18723–18730. [PubMed: 29165498]

(45). Kim KM; Kim HM; Lee WJ; Lee CW; Kim TI; Lee JK; Jeong J; Paek SM; Oh JM Surface Treatment of Silica Nanoparticles for Stable and Charge-controlled Colloidal Silica. Int. J. Nanomed 2014, 9, 29–40.

(46). Packer RA; Rossmeisl JH; Kent MS; Griffin JF; Mazcko C; LeBlanc AK Consensus Recommendations on Standardized Magnetic Resonance Imaging Protocols for Multicenter Canine Brain Tumor Clinical Trials. Vet Radiol Ultrasoun 2018, 59, 261–271.

(47). Garai E; Sensarn S; Zavaleta CL; Van de Sompel D; Loewke NO; Mandella MJ; Gambhir SS; Contag CH High-sensitivity, Real-time, Ratiometric Imaging of Surface-enhanced Raman Scattering Nanoparticles with a Clinically Translatable Raman Endoscope Device. J. Biomed. Opt 2013, 18, 096008. [PubMed: 24008818]

(48). Veterinary Cooperative Oncology Ggroup – Common Terminology Criteria for Adverse Events (VCOG-CTCAE) Following Chemotherapy or Biological Antineoplastic Therapy in Dogs and Cats v1.1. Vet. Comp. Oncol 2016, 14, 417–446. [PubMed: 28530307]

(49). Buetow MP; Buetow PC; Smirniotopoulos JG Typical, Atypical, and Misleading Features in Meningioma. Radiographics 1991, 11, 1087–1106. [PubMed: 1749851]

Author Manuscript Author Manuscript Author Manuscript Author Manuscript

(50). Young BD; Levine JM; Porter BF; Chen-Allen AV; Rossmeisl JH; Platt SR; Kent M; Fosgate GT; Schatzberg SJ Magnetic Resonance Imaging Features of Intracranial Astrocytomas and Oligodendrogliomas in Dogs. Vet Radiol Ultrasoun 2011, 52, 132–141.

(51). Larjavaara S; Mantyla R; Salminen T; Haapasalo H; Raitanen J; Jaaskelainen J; Auvinen A Incidence of Gliomas by Anatomic Location. Neuro-Oncology 2007, 9, 319–325. [PubMed: 17522333]

(52). Wick W; Kuker W Brain Edema in Neurooncology: Radiological Assessment and Management. Oncol. Res. Treat 2004, 27, 261–266.

(53). Perry A; Wesseling P Histologic Classification of Gliomas. Handb Clin Neurol 2016, 134, 71–95. [PubMed: 26948349]

(54). Commins DL; Atkinson RD; Burnett ME Review of Meningioma Histopathology. Neurosurg Focus 2007, 23, E3.

(55). Stummer W Mechanisms of Tumor-related Brain Edema. Neurosurg Focus 2007, 22, 1–7.

(56). Tavares AJ; Poon W; Zhang YN; Dai Q; Besla R; Ding D; Ouyang B; Li A; Chen J; Zheng G; Robbins C; Chan WCW Effect of Removing Kupffer Cells on Nanoparticle Tumor Delivery. Proc. Natl. Acad. Sci. U. S. A 2017, 114, E10871–E10880. [PubMed: 29208719]

Author Manuscript Author Manuscript Author Manuscript Author Manuscript

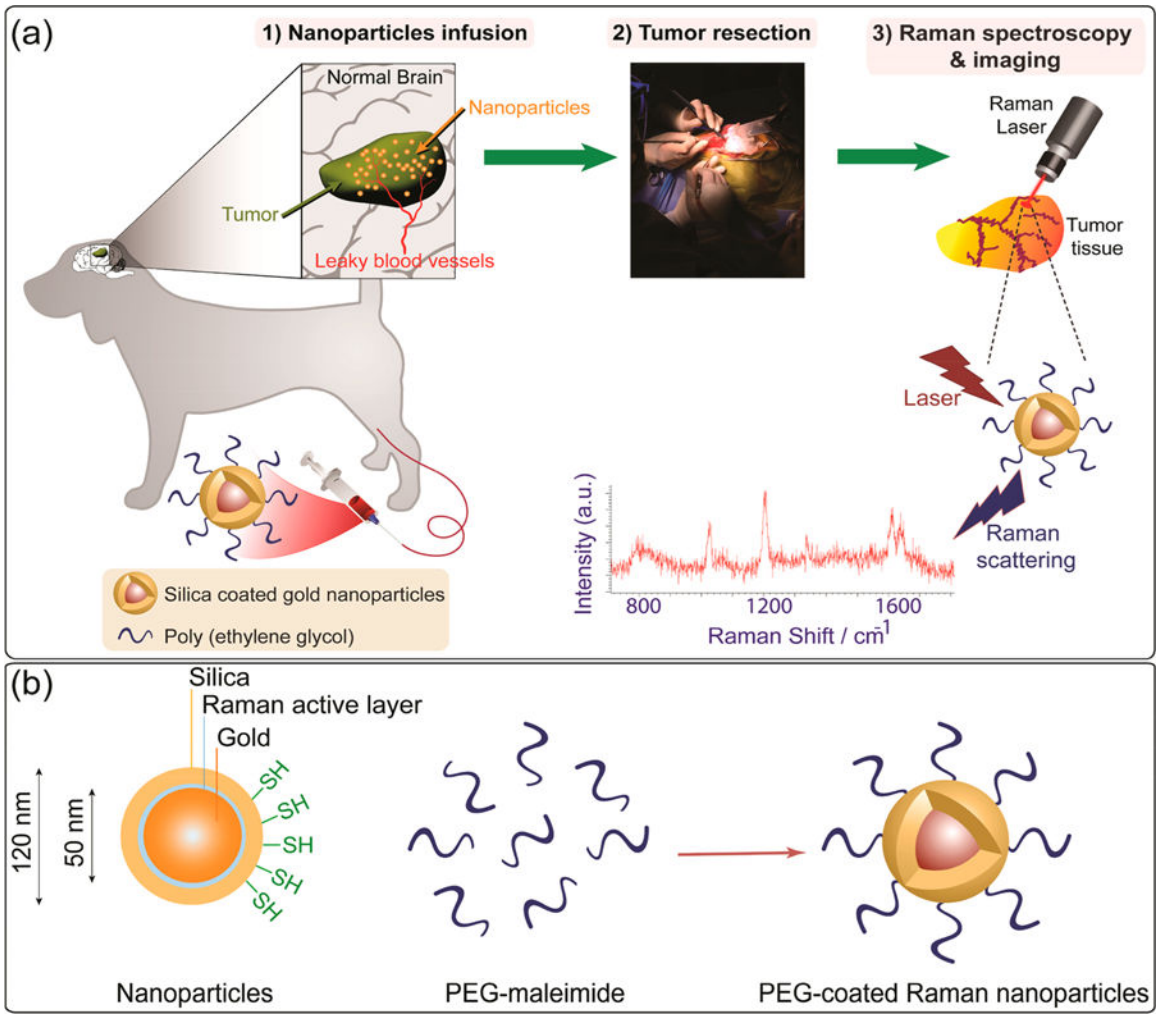

Figure 1.

(a) Schematic showing the overall design of the experiments starting from nanoparticle preparation to intravenous infusion, surgical resection, and analyses. PEGylated silica-coated gold nanoparticles (GNPs) were administered intravenously. GNP extravasation into the brain tumor was confirmed by highly sensitive surface enhanced Raman spectroscopy of the excised tissues, confirming the enhanced permeation and retention (EPR) effect of nanoparticles into naturally occurring spontaneous brain tumors. (b) Schematics showing conjugation of PEG-maleimide to thiol functionalized GNPs to enhance their stability in biological environments (also see Figure S2). Raman reporter molecules were embedded beneath the silica layer and enabled highly sensitive tracking of the GNPs in brain tumors without any additional labeling.

Author Manuscript Author Manuscript Author Manuscript Author Manuscript

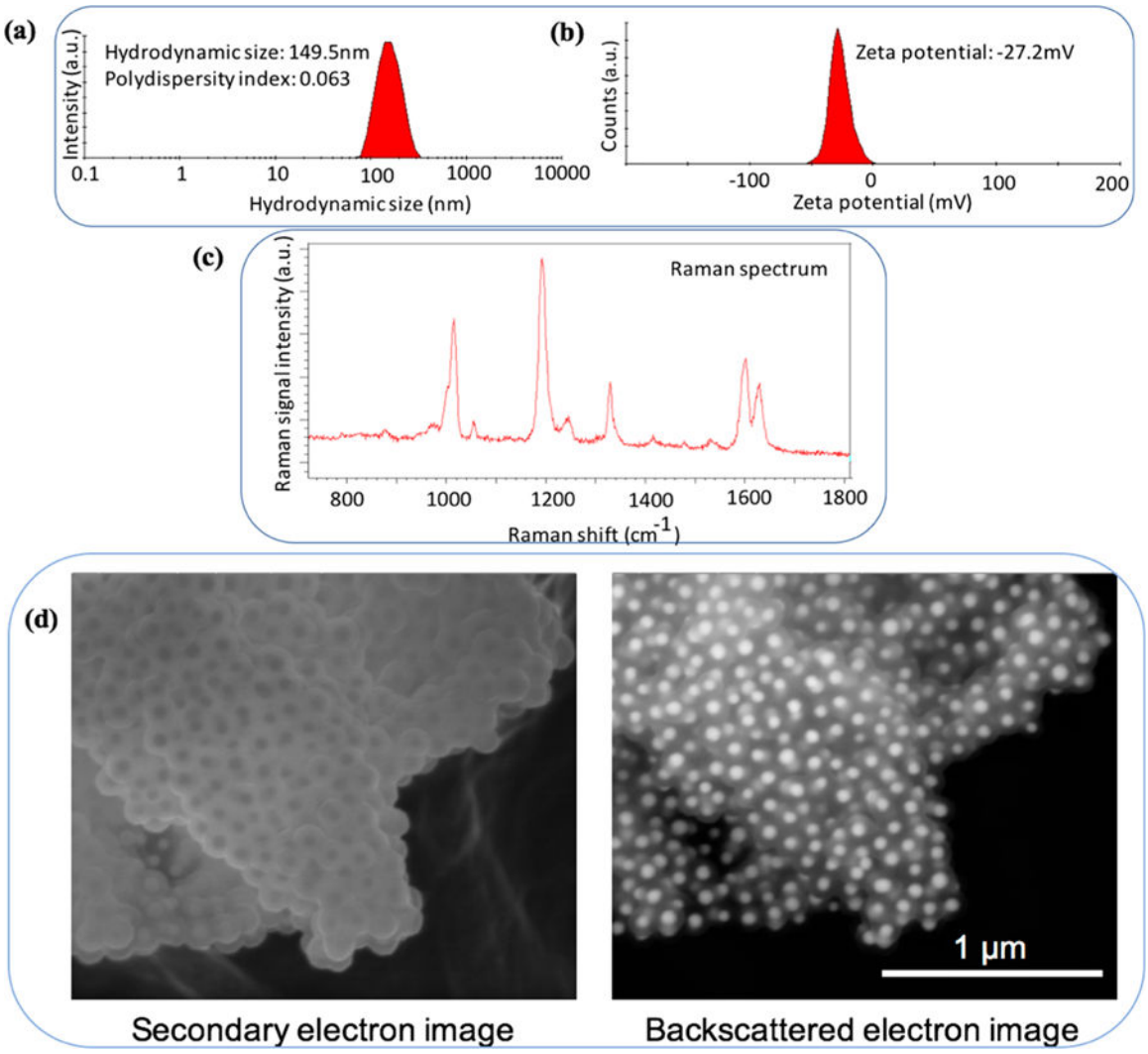

Figure 2.

(a and b) Hydrodynamic size distribution and zeta potential measurements of the PEG coated nanoparticles, showing an average size of ~150 nm (PDI: 0.06) and charge of ~−27 mV. The volume and number percentage diagrams are shown in Figure S3. The dynamic light scattering (DLS) measurements were performed in D5W solution. (c) Raman spectrum of the PEG coated nanoparticles. (d) Secondary and backscattered scanning electronic microscopy (SEM) images showing the uniform core?shell structure of silica coated gold nanoparticles. Stable and uniform silica layer ensured tight proximity of Raman reporter molecules to the surface of gold nanoparticles for surface plasmon resonance. Gold cores can be seen with darker and brighter contrasts in secondary and backscattering images, respectively.

Author Manuscript Author Manuscript Author Manuscript Author Manuscript

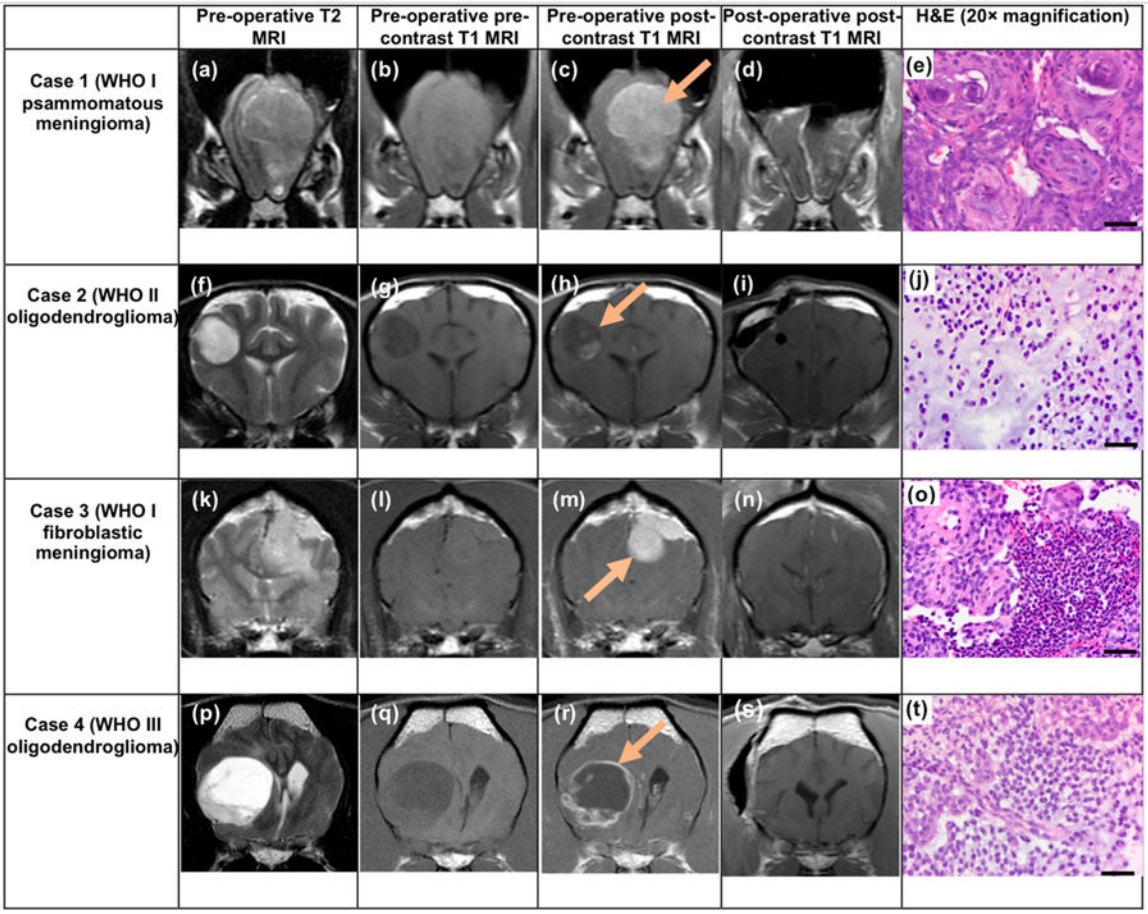

Figure 3.

Panel shows MR imaging for all four cases consisting of three preoperative transverse MRI scans (T2-, precontrast T1-, and postcontrast T1-weighted), the postoperative transverse postcontrast T1-weighted (T1W) MRI, and representative histology (H&E) images. T1W MRI scans were acquired before and after administration of gadolinium contrast (also see Figure S6 and the 3D MRI Supplementary Videos). The difference between the pre- and postcontrast T1W MRI scans (the bright area visible after administration of contrast that was not visible prior to contrast administration) indicates the contrast-enhancing tumor that contained hypervascularity or breakdown of the blood?brain barrier. Arrows in preoperative postcontrast T1W images indicate brain tumor areas in each case. T2 hyperintensity involving brain parenchyma beyond the margins of the mass likely represent vasogenic edema (high water content; panels k and p). Histology of the H&E stained tissue sections obtained from the surgery shows characteristics of psammomatous and fibroblastic meningiomas in Cases 1 and 3, respectively, and grade II and III oligodendroglioma in Cases 2 and 4, respectively. H&E = hematoxylin and eosin, MRI = magnetic resonance imaging, WHO = World Health Organization. H&E scale bars = 50 μm.

Author Manuscript Author Manuscript Author Manuscript Author Manuscript

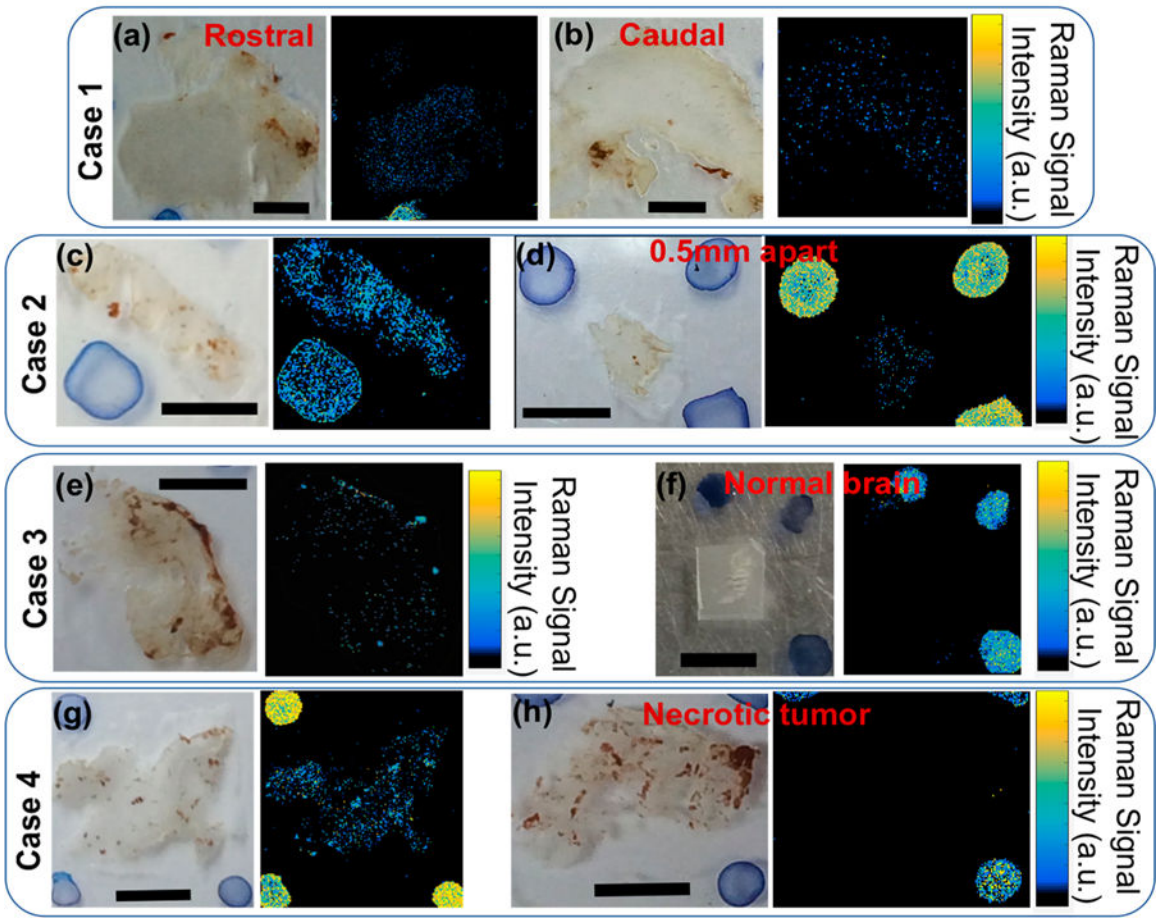

Figure 4.

White light and the counterpart Raman images of the tumor tissue sections (100 μm thick) resected from Cases 1, 2, 3, and 4, respectively. Sensitivity of the Raman microscopy helped detect traces of GNPs embedded in these tissue sections accurately and generate 2D maps of GNP distribution in tissues (also see Figures S7–S10). Comparing the images obtained from each case shows that GNPs had a heterogeneous distribution through the tumors. (a and b) Representative images obtained from caudal and rostral regions of the psammomatous meningioma in Case 1. (c and d) Images from oligodendroglioma tumor sections, where section (d) was cut at 0.5 mm from section (c). (e) Image of the fibroblastic meningioma tumor section in comparison with an area of normal brain (f) surrounding the resected tumor. This latter case supports that GNPs extravasated into the tumor only, with no detectable uptake in normal brain tissues. Finally, (g and h) Representative images generated from a tissue section cut from the margins of the tumor and central necrotic part. Blue spots in white light images are different mixtures of GNPs and Trypan Blue, used as fiducials for image reconstruction and accurate orientation adjustments. Scale bars in all images = 3 mm.

Author Manuscript Author Manuscript Author Manuscript Author Manuscript

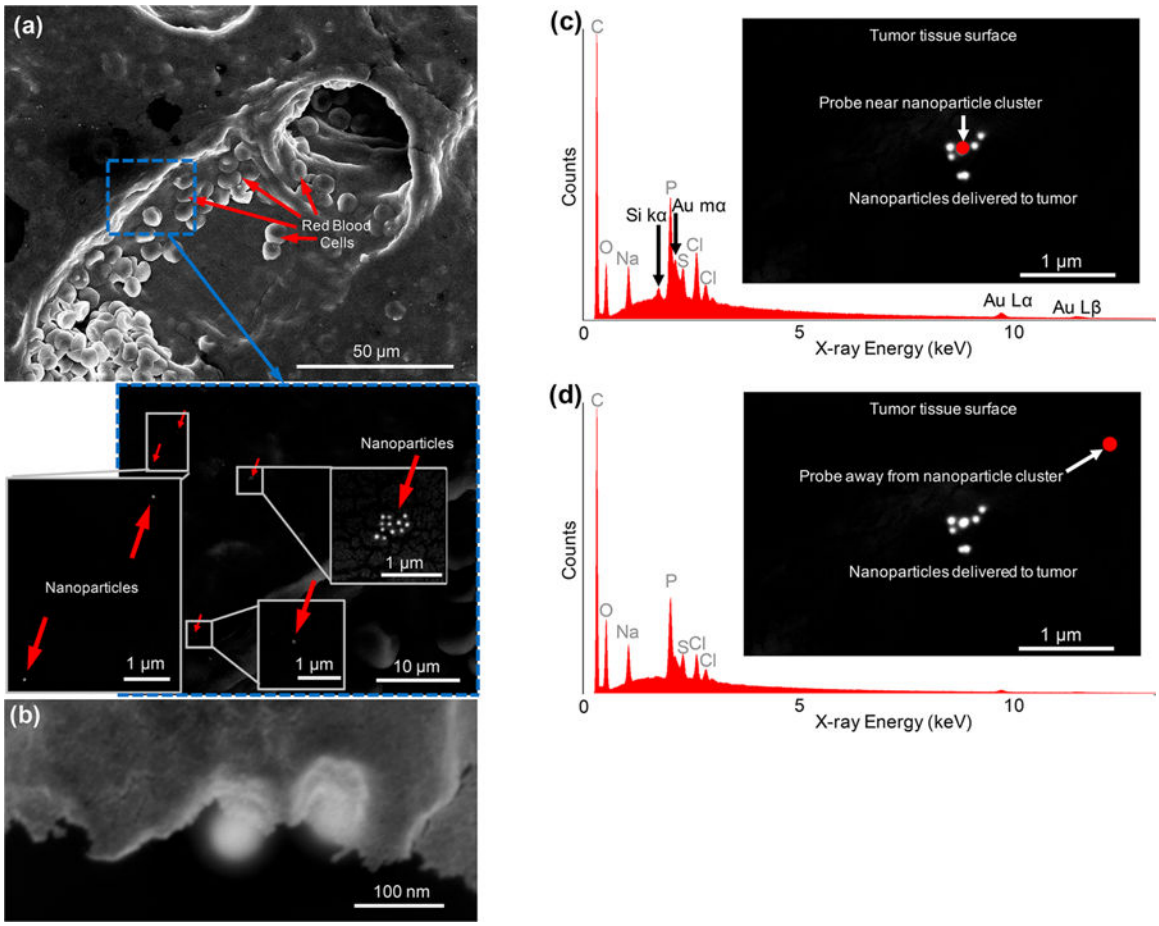

Figure 5.

SEM images (a and b) and energy-dispersive X-ray spectroscopy (c and d) of a brain tumor section (100 μm-thick section) showing extravasated nanoparticles (GNPs) adjacent to a blood vessel inside the meningioma tumor (Case 1). (a) Secondary electron images are generated based on the contrast on the surface of the tissues, providing topographical information about the features on the surface, such as presence of a blood vessel and red blood cells that were visible on histological preparations. Higher magnification backscattered electron image shows individual NPs as bright spots adjacent to the blood vessel since gold generates a strong bright contrast in the SEM backscattered mode. This helps to distinguish GNPs from the tissue (also see Figures S13 and S14 for additional SEM analyses of the tissues). (b) Backscattered electron image of a cross section of the tumor tissue, showing two individual NPs embedded into the tumor. (c) Energy dispersive X-ray spectroscopy elemental analysis of the bright spots seen in backscattered mode showed specific Si K? and Au M? peaks from silicon (Si) and gold (Au) elements, confirming the administration of silica-coated gold nanoparticles (GNPs). These specific Si and Au peaks disappeared when the electron beam was shifted away from these bright spots (d). The location of the electron beam is shown with a red circle in (c) and (d). These specific Si and Au peaks disappeared when the electron beam was shifted away from these bright spots (d). The location of the electron beam is shown with a red circle in (c) and (d).

Author Manuscript Author Manuscript Author Manuscript Author Manuscript

Table 1.

Clinical and Pathology Summary of Four Recruited Dog Cases with Different Types of Primary Brain Tumors[a]

case no.	dog breed	age (y)	weight (kg)	pathology diagnosis	WHO grade	GNP dose (pmol)
1	Border Collie mix	13	24.7	psammomatous meningioma	I	24.7
2	Boston Terrier	7	8.7	oligodendroglioma	II	8.7
3	Australian Cattle and Border Collie mix	8	20.3	fibroblastic meningioma	I	20.3
4	French Bulldog	4	17	oligodendroglioma	III	17

[a]Dosage of the injected gold nanoparticles (GNP) was adjusted to 0.5 pmol of the GNPs per kg of body weight for each subject. GNP = gold nanoparticles, WHO = World Health Organization.

ACS Nano. Author manuscript; available in PMC 2019 June 19.